Supplementary Figures

Supplementary Figure 1: Viral labeling of granule cells with dTomato and GCaMP3. **A**. Tissue sections from OB of mice injected with AAV2/1 virus carrying genes for GCaMP3 and dTomato (insert sequence schematized on top). Red and green channels are native fluorescence from the two proteins, and DAPI signals (blue) highlight nuclei of cells. Note dense signal in the external plexiform layer (EPL), where the apical dendrites of GCs reside, and in the granule cell layer (GCL). Mitral cells are largely unlabeled and are seen as ghosts in the fluorescence images. **B**. Cre-dependent expression of dTomato and GCaMP3 in a VGAT-Cre mouse. Tissue sections show excellent colocalization of dTomato and GABA, with no expression in GABA-negative mitral cells.

Supplementary Figure 2: **A**. Scatter plot of odor-evoked fluorescence signals across two trials plotted for >2500 GC-odor pairs. A linear fit and the 95% confidence intervals are shown in red. The confidence interval is around 8% of the mean. **B**. The maximum response of each GC (across the 20 odors used) did not correlate with the resting fluorescence ($p = 0.134$). This suggests that resting fluorescence (for example, due to expression levels) is not the main determinant the magnitude of responses. **C**. Blocking inhibition with bicuculline reveals that most GCs can become activated. Each column represents the time course of fluorescence intensity in 150 GCs during odor stimulation with two odors (ethyl tiglate at left and 2-methoxypyrazine at right). GCs are rank ordered in decreasing response amplitude under control conditions. Note that after bicuculline infusion into the OB, most of the GCs respond to ethyl tiglate. Therefore, the lack of responses of many of the labeled GCs under control conditions is not due to an inability of these neurons to increase their fluorescence – for example, due to nonspecific loss of the indicator's calcium reporting ability. **D**. The percent of non-responding GCs within the imaged region (calculated as described in Methods) was high

for most odorants under control conditions (blue), but went down significantly for most odors after bicuculline infusion (red).

Supplementary Figure 3: **A**. Responses of GCs as measured with GCaMP5, which has better sensitivity than GCaMP3. The average responses to 20 odors for each GC was arranged in descending order, and the resulting "tuning curves" averaged across 150 GCs from 2 experiments (red). For comparison, a null distribution was calculated from the baseline fluorescence fluctuations (black). From this data, we estimated that a GC responded to 6 odors on average (compared to 3 estimated with GCaMP3). **B**. The overall population activity of GCs for a given odor, measured with GCaMP5, was also highly correlated with the fraction of glomeruli activated by that odor. This confirms the findings using GCaMP3.

Supplementary Figure 4: Responses of GCs in awake mice were stronger, but the basic findings from anesthetized animals hold. **A**. Imaged regions from the same mouse under anesthesia and when the mouse was awake. Although the two regions are different, they are very close to each other. It was technically difficult to return to the same region for the two imaging conditions. **B**. Time course of responses 50 GCs to two different odorants under anesthetized and awake condtions. GCs were more responsive in awake animals. **C**. Average tuning curves of GCs to 20 odors estimated by rank ordering odor responses for individual GCs and averaging them under anesthetized (red) and awake (blue) conditions. GC responsiveness to odors is clearly higher in awake mice. **D**. The strong correlation between the extent of glomerular activation and the overall population activity of GCs is preserved in awake mice. **E**. Average responses of 50 GCs to increasing concentration of an odorant (allyl tiglate). GCs are rank ordered by the decreasing responsivity to the highest concentration. F. The average responses of all cells (black, dashed line) shows gradual increase in responses with increasing concentration, which is also seen for GCs with the strongest responses to the highest

concentration (blue). However, responses of 5 GCs in the middle ranks revealed non-monotonic behavior (red), just as we observed for recordings in anesthetized animals.

Supplementary Figure 5: **A**. The relation between the fraction of glomeruli activated by an odor and the population sparseness of GCs (calculated as described in Methods). This experiment was in VGAT-Cre mice. The correlation coefficient was 0.83 and $p < 0.01$. **B**. Lifetime sparseness (calculated as described in Methods) across a population of GCs. Some measures for GC selectivity relies on using thresholds to define responses, making those measures sensitive to noise and other factors. Lifetime sparseness does not use any threshold for defining a response, and indicates how selective an individual neuron is to the range of stimuli. In our definition a value of 1 indicates equal responses to all stimuli and a value close to 0 indicates a very sparse code. We found that the lifetime sparseness varied from cell to cell, with an average value of 0.24 +/- 0.18 (N = 5 experiments, 637 GCs).

Supplementary Figure 6: **A**. Responses of 45 glomeruli from 2 OMP-GCaMP3 mice to increasing concentrations of allyl tiglate. Glomeruli were rank-ordered in decreasing response amplitudes for the highest concentration (right most panel), and the glomerular identities were then matched for the rest of the concentrations. **B**. Relation between responses and odor concentration for 6 glomeruli. The glomeruli were chosen to span a range of responses to the highest odor concentration (note different scales on the Y axis). **C**. Average response amplitudes for 3 glomeruli in the top, middle and bottom ranges of response amplitudes to the highest concentration. Note that all responses were monotonically increasing, unlike what was seen for GCs.

Supplementary Figure 7: Distribution of average pairwise separation of GCs randomly sampled from all the cells in the imaged region. From a population of ~150 cells in an

experiment, 3, 5 or 20 cells were randomly chosen and their average pairwise separation calculated. This randomly sampling was repeated for a total of 1000 simulations. Note that the distribution became wider when only a few cells were sampled, but they were always symmetrically spread around the mean value.

Supplementary Figure 8: **A**. Responses 80 GC dendritic segments to increasing concentrations of allyl tiglate. Dendrites were rank-ordered in decreasing response amplitudes for the highest concentration, and the dendritic identities were then matched for the rest of the concentrations. **B**. Average response amplitudes for 5 dendritic segments in the top, middle and bottom ranges of response amplitudes to the highest concentration. Note that all responses were monotonically increasing, unlike what was seen for GC somata.

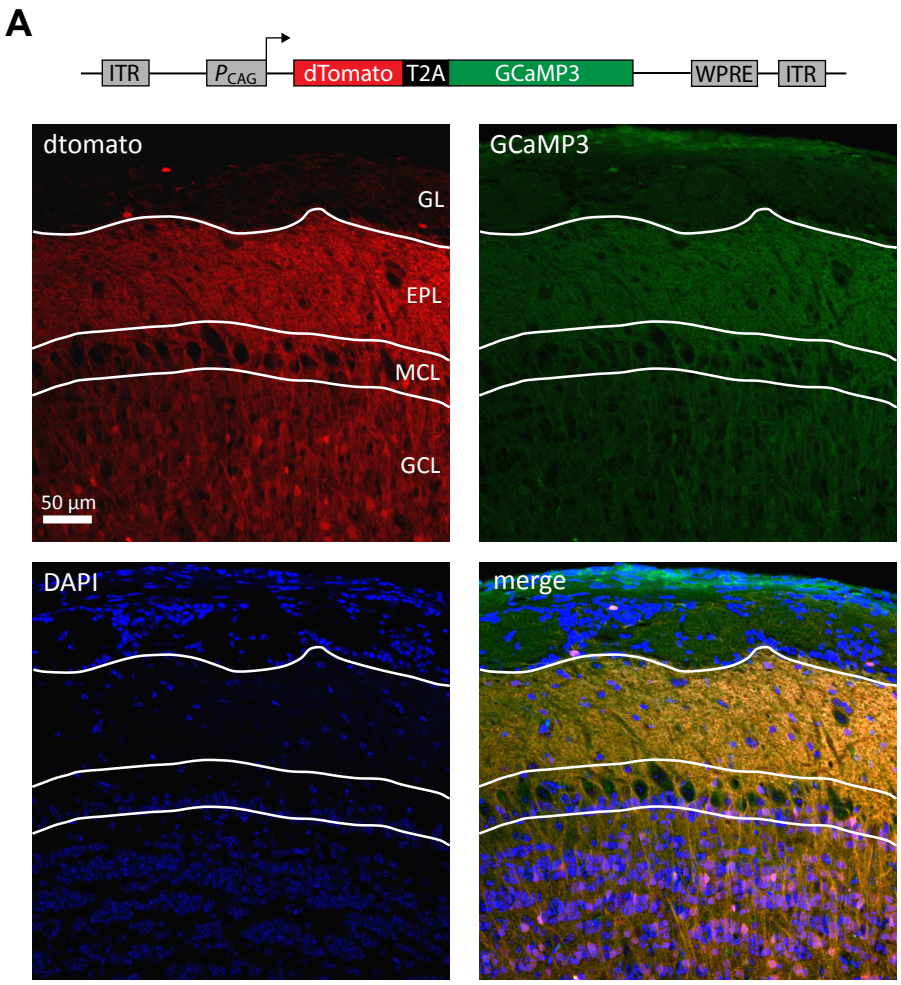
A
ITR
P_{CAG}
dTomato
T2A
GCaMP3
WPRE
ITR
dtomato
GL
EPL
MCL
GCL
50 µm
GCaMP3
DAPI
merge
B
dtomato
EPL
MCL
GCL
50 µm
GABA
DAPI
merge

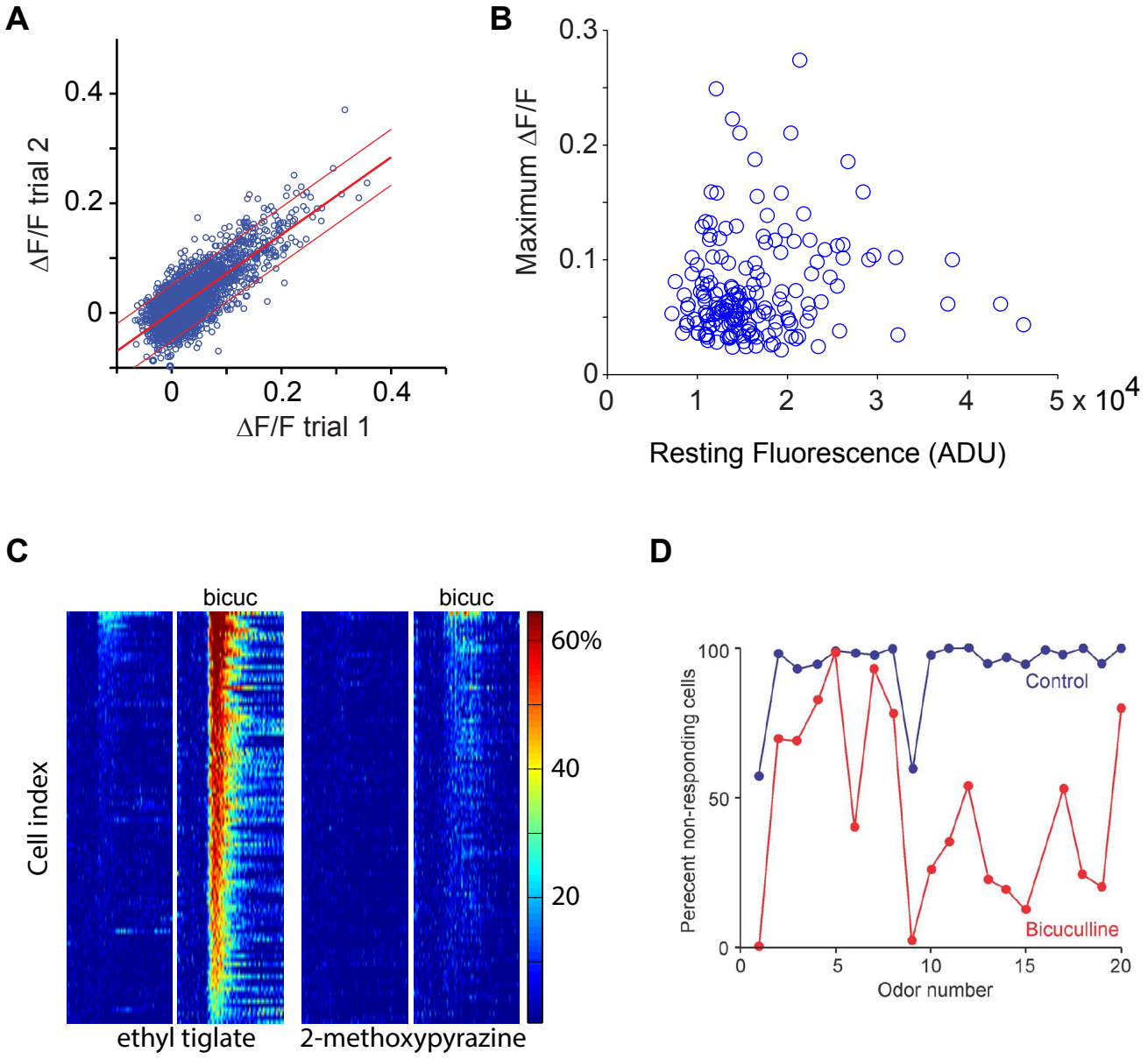
A
0.4
0.2
0
ΔF/F trial 2
0
0.2
0.4
ΔF/F trial 1
B
0.3
0.2
0.1
0
Maximum ΔF/F
0
1
2
3
4
5 x 10^4
Resting Fluorescence (ADU)
C
bicuc
bicuc
Cell index
60%
40
20
ethyl tiglate
2-methoxypyrazine
D
100
50
0
Perecent non-responding cells
Control
Bicuculline
0
5
10
15
20
Odor number

Supplementary Figure 3

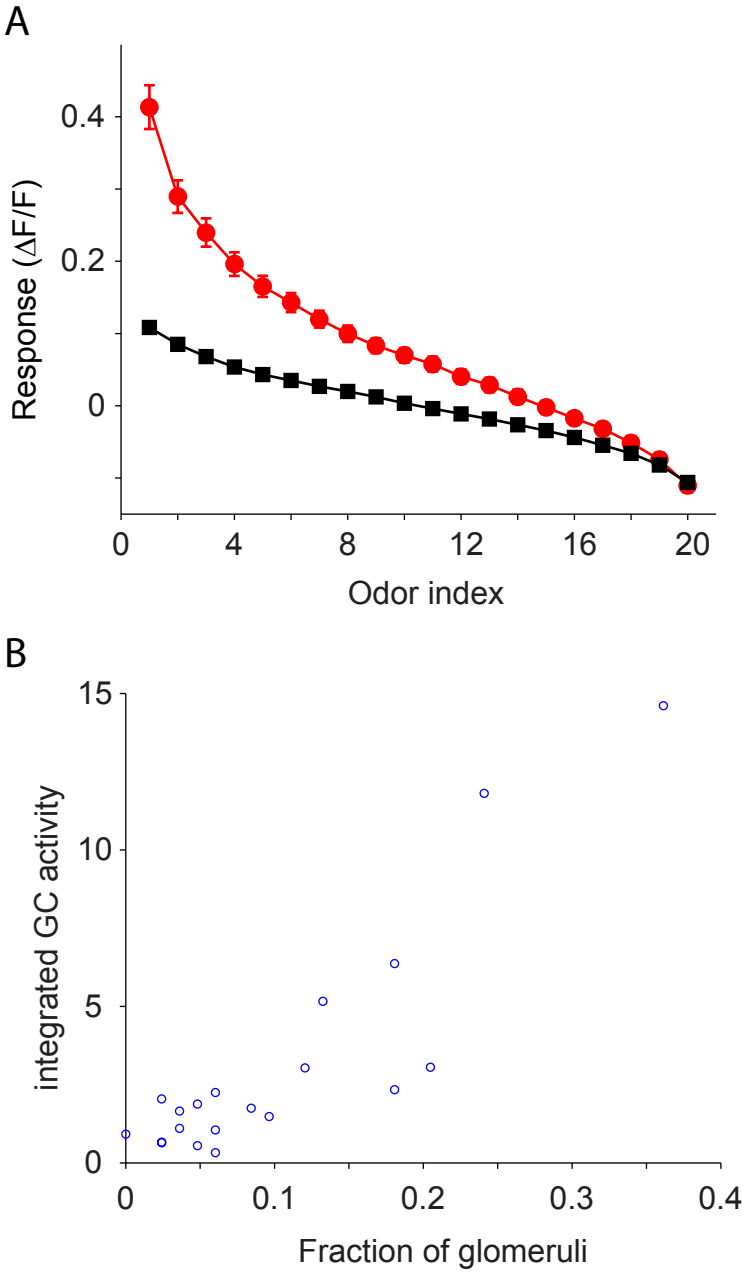

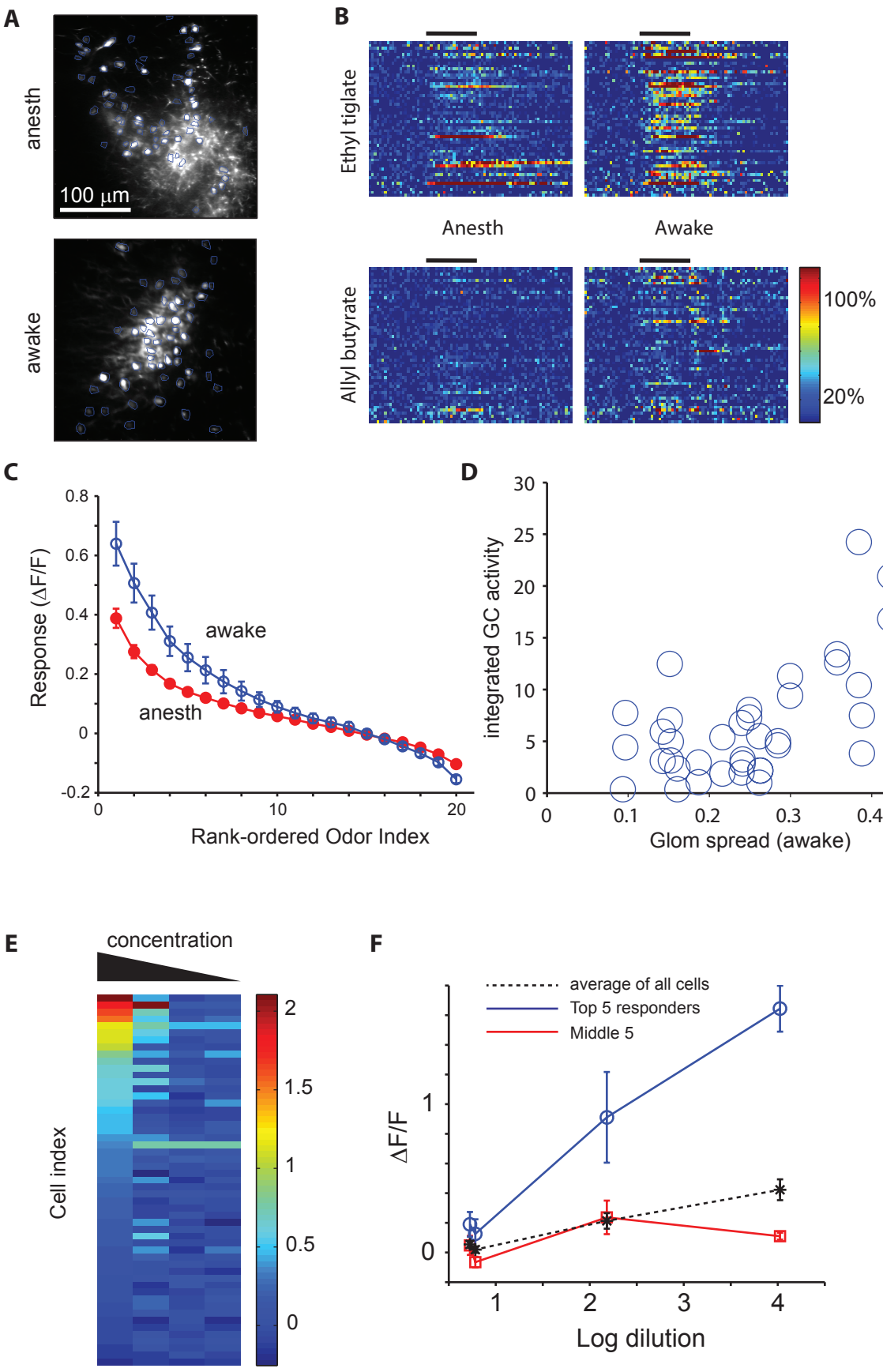
A
anesth
awake
100 µm
B
Ethyl tiglate
Allyl butyrate
Anesth
Awake
100%
20%
C
Response (ΔF/F)
awake
anesth
Rank-ordered Odor Index
D
integrated GC activity
Glom spread (awake)
E
concentration
Cell index
F
average of all cells
Top 5 responders
Middle 5
ΔF/F
Log dilution

Supplementary Figure 5

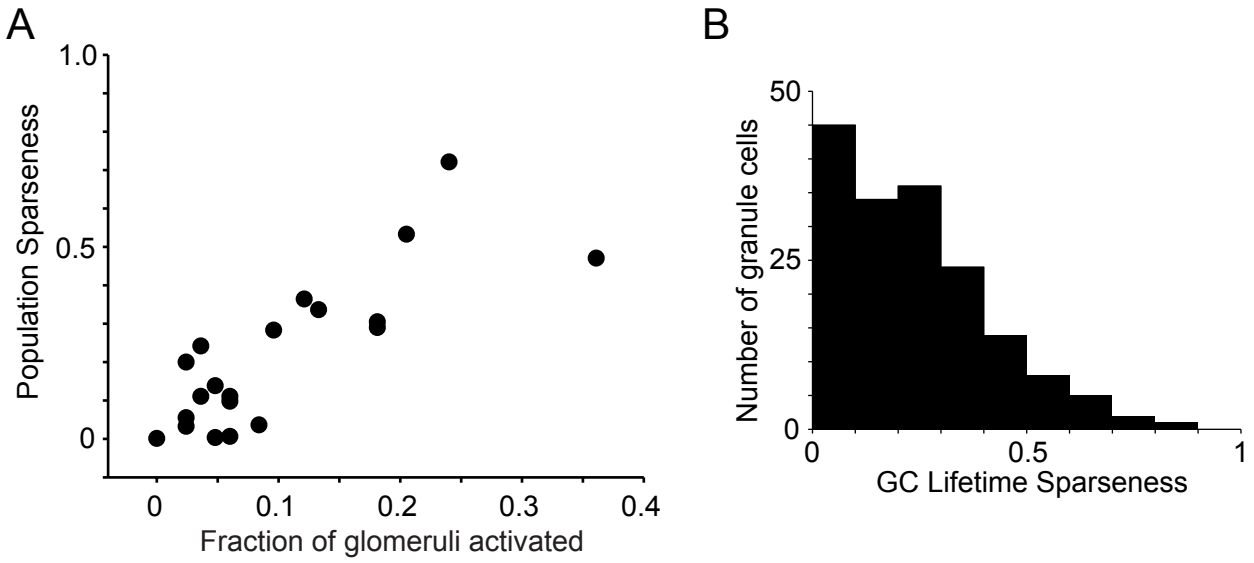

Supplementary Figure 6

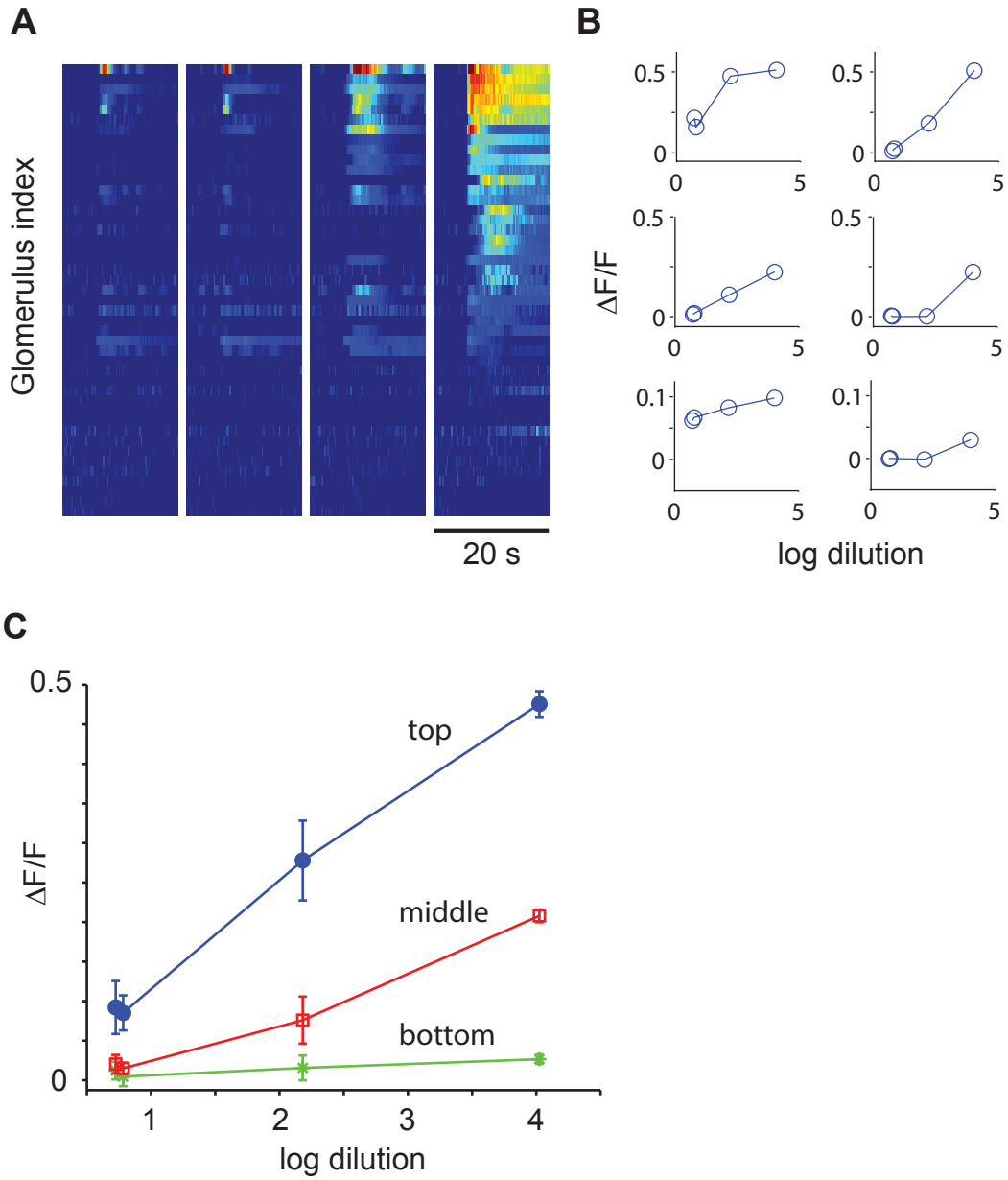

Supplementary Figure 7

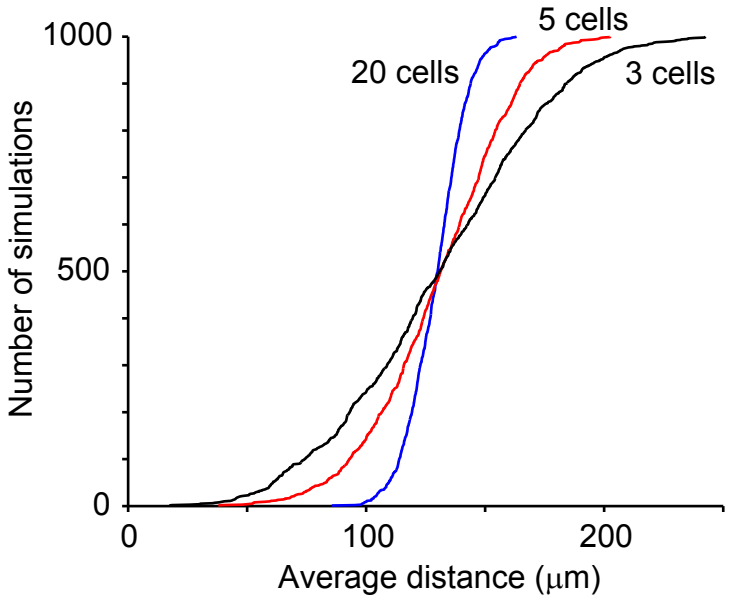

Supplementary Figure 8